IEEE Photonics Journal
An IEEE Photonics Society Publication

Open Access

OLED Panel Radiation Pattern and Its Impact on VLC Channel Characteristics

Volume 10, Number 2, April 2018

Hanjie Chen
Zhengyuan Xu

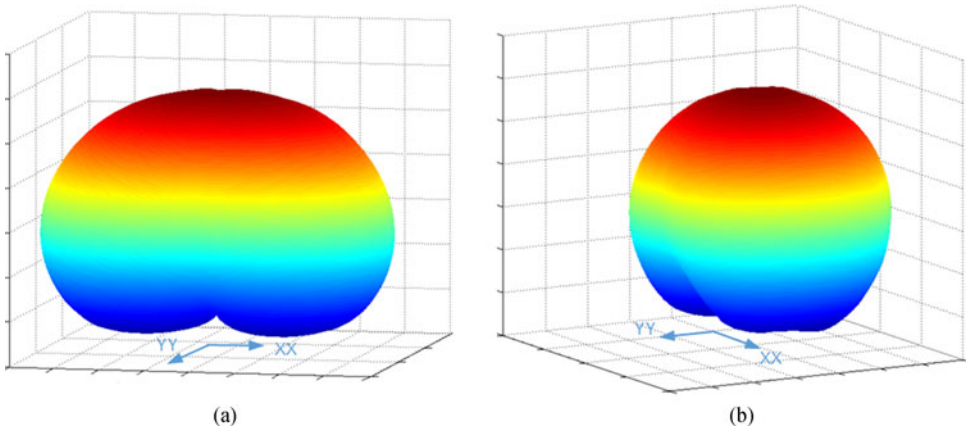

(a) (b)

DOI: 10.1109/JPHOT.2017.2774241
1943-0655 © 2017 IEEE

IEEE photonics SOCIETY

IEEE

OLED Panel Radiation Pattern and Its Impact on VLC Channel Characteristics

Hanjie Chen [1] **and Zhengyuan Xu** [1,2]

[1]Key Laboratory of Wireless-Optical Communications, Chinese Academy of Sciences, School of Information Science and Technology, University of Science and Technology of China, Hefei 230027, China
[2]Shenzhen Graduate School, Tsinghua University, Shenzhen 518055, China

DOI:10.1109/JPHOT.2017.2774241

Manuscript received October 7, 2017; revised November 4, 2017; accepted November 13, 2017. Date of publication November 16, 2017; date of current version February 28, 2018. This work was supported in part by the National Key Basic Research Program of China under Grant 2013CB329201, in part by the Key Program of National Natural Science Foundation of China under Grant 61631018, in part by the Key Research Program of Frontier Sciences of CAS under Grant QYZDY-SSW-JSC003, in part by the Key Project in Science and Technology of Guangdong Province under Grant 2014B010119001, and in part by the Shenzhen Peacock Plan under Grant 1108170036003286. Corresponding author: Zhengyuan Xu (e-mail: xuzy@ustc.edu.cn).

Abstract: Organic light-emitting diodes (OLEDs) show several attractive features superior to traditional semiconductor LEDs for visible light communication (VLC). This paper experimentally tests and models the radiation pattern of a bent OLED panel for the first time. Different from a Lambertian radiation pattern, we propose an improved analytic mixed Gaussian model to describe the rotational radiation asymmetry, whose parameter values are found by applying an expectation-maximization algorithm for curve fitting with measurements. The OLED radiation pattern is observed to show strong directionality along the bent axes. Its impact on VLC channel characteristics is further studied. Compared with the Lambertian source, the OLED source is more flexible in radiation pattern control and shows advantages in smaller root mean square delay spread and optical path loss.

Index Terms: Organic LED, radiation pattern, visible light communication (VLC), channel characteristics.

1. Introduction

As new light sources, organic light-emitting diodes (OLEDs) have been applied to visible light communication (VLC) [1]–[4]. Compared with traditional semiconductor LEDs, OLEDs have several attractive features, including flexibility, easy integration and fabrication, rich colors and wide beaming angle. Their optimum operating voltage, bandwidth and spectrum have been studied in detail [5]–[7]. Nevertheless, the lower cut-off frequency of OLEDs is a key disadvantage, which limits the transmission data rate compared with an LED-based system. Thus a lot of efforts have been made to increase the data rate of an OLED-based VLC system. Different advanced communication and signal processing techniques have been proposed [8]–[10], including equalization, multiple-input-multiple-output (MIMO), and orthogonal frequency division multiplexing (OFDM). Those techniques have led to a significant breakthrough in data rate over the past years [11]–[14], from Mbps to tens of Mbps.

The radiation pattern of a light source has an important impact on VLC channel characteristics, and consequently influences the VLC system performance [15]. The need for practical lighting

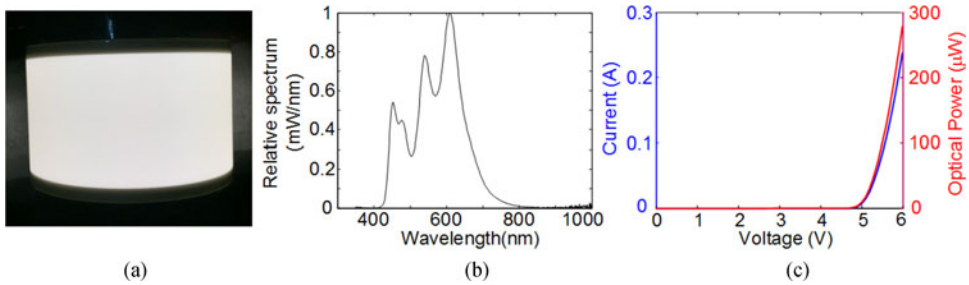

Fig. 1. OLED panel and its characteristics. (a) Photograph. (b) Normalized optical spectrum. (c) I-V and P-V curves.

designs is growing and radiation patterns of traditional LEDs have been modeled based on a general Lambertian representation [16]. To the best of our knowledge, there is rarely any research on OLED radiation pattern, especially related to flexibility. OLEDs are usually encased in glass substrates to avoid exposure to air, which hides their big advantages in flexibility.

In this paper, we test the characteristics of a flexible OLED panel by bending the panel in different curvatures. Corresponding radiation patterns describing the angular distribution of the light intensity are studied. As a kind of flexible and uniformly illuminated surface light source, the OLED panel has a larger semiangle at half intensity with a larger curvature in the bent direction, superior to the generalized Lambertian pattern for a conventional LED source. As the bent OLED no longer presents a Lambertian radiation pattern, we propose an improved mixed Gaussian analytic representation to describe the rotational asymmetry of the light emitted from the OLED. The probability distribution function (PDF) of the measured optical intensity shows a good fitting with mixed Gaussian distribution, whose model parameters can be determined by an expectation-maximization (EM) algorithm [17]. The undetermined unknown parameters in the proposed model are optimized by maximizing the joint probability of the estimated optical intensity based on maximum likelihood (ML) estimation. The analytic model can fit the experimental OLED radiation pattern well according to our results.

With the OLED panel model, the characteristics of the OLED-based VLC channel are further evaluated. In a typical indoor scenario, the light source is often assumed to be the Lambertian pattern, which is rotational symmetric and has the broadest angular characteristics compared with other sources. However, the OLED has a larger semiangle in the bent direction, which can lead to better channel characteristics. We study the channel characteristics, including root mean square (RMS) delay spread and optical path loss (OPL) through simulation [15]. Numerically, both the RMS delay spread and the OPL of the OLED are less than those of the Lambertian pattern. The results jointly indicate that the OLED source can bring benefits to VLC systems with better channel characteristics and reduced inter-symbol interference (ISI) induced by multipath dispersion. The flexibility of the OLED provides another degree of freedom to design and performance optimization for a VLC system.

The rest of this paper is organized as follows. In Section II, we examine the properties of the OLED panel and propose an improved analytic representation to model the radiation pattern. Section III further studies the channel characteristics based on the model. Finally, Section IV concludes the paper.

2. OLED Radiation Pattern

We adopt a customized rectangular OLED panel produced by a local manufacturer in our experiments, as showed in Fig. 1(a). We examine the electrical and optical properties of the adopted device and then model the radiation pattern for subsequent studies on channel characteristics.

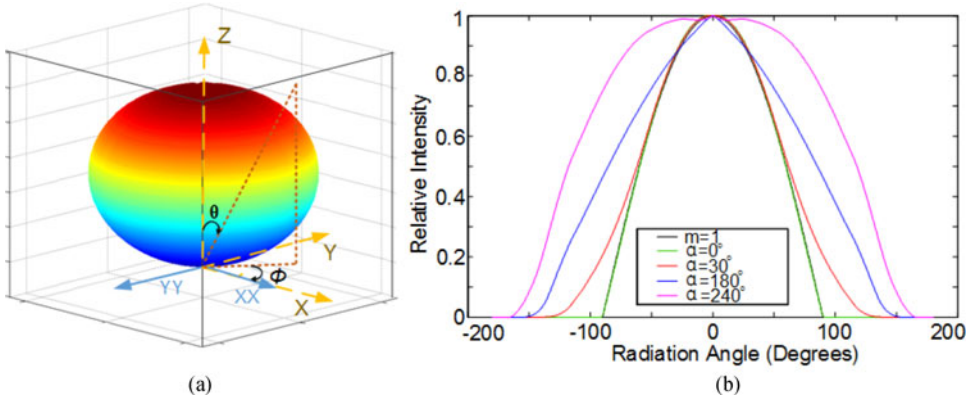

Fig. 2. OLED radiation pattern. (a) Three-dimensional radiation pattern when $\alpha = 0°$. (b) Two-dimensional intensity pattern of XX direction.

2.1 OLED Characteristics

The luminous area of the OLED panel adopted in the experiment is 5×20 cm^2. We examine the normalized optical spectrum under a normal bias voltage by a spectrum analysis system (EVERFINE Integrating Sphere). The peak wavelengths are found at 452 nm, 477 nm, 540 nm, and 610 nm, as Fig. 1(b) shows. Red and green components dominate the light source. Its measured current-voltage (I-V) and power-voltage (P-V) curves are depicted in Fig. 1(c), where I is the forward current, V is the bias voltage, and P is the output optical power. The bias voltage leading to the maximum quasi-linear operation range is found to be about 5.6 V. This working voltage is fixed in the subsequent experiments.

The radiation patterns of the panel are tested in different curvatures. As the panel follows a rectangular shape, we bend it along the minor axis. The curvature of the panel is described by angle α between two tangent lines of two side cambers along the major bending axis perpendicular to the minor bending axis. Without bending ($\alpha = 0°$), the radiation pattern is almost the same as the standard Lambertian pattern (m $= 1$) [18] as Fig. 2(a) shows. As the curvature increases from slight to extreme bending, α increases passing through 0° (flat surface), 90° (quarter circular surface), 180° (half circular surface), 270° (3 quarter circular surface), till 360° (full circular surface). In a coordinate system centered in the panel, θ is the polar angle ranging from 0° to 180° and ϕ is the azimuthal angle ranging from 0° to 360°. We define the XX cross section corresponding to $\phi = 0°$ or 180°, and YY cross section corresponding to $\phi = 90°$ or 270°. When the panel is bent, its radiation pattern is rotationally asymmetric. Fig. 2(b) plots the spatial intensity distribution of XX azimuthal direction which is directly affected by curving. When $\alpha = 0°$, the intensity pattern nearly overlaps the m $= 1$ Lambertian pattern with a semiangle ($\theta_{\frac{1}{2}}$) at 120°. As α increases from 0° to 240°, $\theta_{\frac{1}{2}}$ increases from 120° to 240°, which means the panel is bent to a large extent to go far beyond the maximum semiangle of the generalized Lambertian pattern. It also indicates that an OLED-based VLC system can significantly benefit from this broader irradiation range for a flexible coverage of a communication area.

2.2 Radiation Pattern Modeling

As the OLED panel is bent along one axis, the radiation pattern is rotationally asymmetric, especially in two perpendicular azimuthal directions (XX and YY). The Lambertian pattern expressed by univariate equation only related to θ is not applicable to describe the OLED radiation pattern [16]. The OLED panel can be regarded as an aggregation of massive tiny Lambertian light sources. The light pattern is a combination of Lambertian functions and Gaussian functions generated by diffuse reflections and diffuse refractions [19], [20]. For a given α, we propose an improved analytic

representation with azimuthal angle ϕ additionally introduced to fit the experimental data

$$I(\theta,\phi)=\sum_{i=1}^{U}a_i\exp\left\{-\left[\frac{(\theta-b_i)^2\cos^2\phi}{c_i^2}+\frac{(\theta-d_i)^2\sin^2\phi}{e_i^2}\right]\right\}, \tag{1}$$

where $I(\theta,\phi)$ is relative optical intensity, a_i, b_i, c_i, d_i and e_i are undetermined model parameters, and U is the order. Assume M samples $I(\theta_p,\phi_q)$ $(p=1,2,\ldots,P;\ q=1,2,\ldots,Q)$ are available from measurements, where P is the number of θ samples, Q is the number of ϕ samples, and $M=P\times Q$.

In order to find the model parameters for a given α, we conduct extensive measurements corresponding to $\theta\in(0°,\ 180°\ )$ at a step size of 0.5°, and $\phi\in(0°\ 360°)$ at a step size of 5°. We choose the PDF of all measured $I(\theta,\phi)$ as a performance metric for comparison between model and experiments, which captures the overall effect of modeling for the whole ranges of angular settings. We consider the following mixed Gaussian distribution for PDF modeling

$$\mathcal{P}(I(\theta,\phi))=\sum_{k=1}^{K}p(k)p(I|\mu_k,\sigma_k^2)=\sum_{k=1}^{K}p(k)\mathcal{N}(I|\mu_k,\sigma_k^2), \tag{2}$$

where K is the number of components and $p(k)$ is the proportion of the kth Gaussian distribution. $\mathcal{N}(I|\mu_k,\sigma_k^2)$ is the Gaussian distribution function with mean μ_k and variance σ_k^2. The parameters K, $p(k)$, μ_k and σ_k in PDF can be determined by ML estimation from totally M samples, that is to maximize the log-likelihood function

$$\max\sum_{p,q}\log\mathcal{P}(I(\theta_p,\phi_q))=\max\sum_{p,q}\log\sum_{k=1}^{K}p(k)\mathcal{N}(I(\theta_p,\phi_q)|\mu_k,\sigma_k^2). \tag{3}$$

To solve this highly nonlinear optimization problem, we adopt the EM algorithm [17]. The first step is to calculate the probability of each sample data generated by each Gaussian distribution. For $I(\theta_p,\phi_q)$, the probability of it being generated by the kth Gaussian distribution is

$$\gamma(p,q,k)=\frac{p(k)\mathcal{N}(I(\theta_p,\phi_q)|\mu_k,\sigma_k^2)}{\sum_{j=1}^{K}p(j)\mathcal{N}(I(\theta_p,\phi_q)|\mu_j,\sigma_j^2)}. \tag{4}$$

It is calculated by iterations with μ_k and σ_k^2 obtained from the previous iteration results or initial values (at the beginning of iteration). We consider that the kth Gaussian distribution produces $\gamma(p,q,k)I(\theta_p,\phi_q)$. Then the parameters can be updated as

$$\mu_k=\frac{\sum_{p,q}\gamma(p,q,k)I(\theta_p,\phi_q)}{\sum_{p,q}\gamma(p,q,k)},\ \sigma_k^2=\frac{\sum_{p,q}\gamma(p,q,k)(I(\theta_p,\phi_q)-\mu_k)^2}{\sum_{p,q}\gamma(p,q,k)},\ p(k)=\frac{\sum_{p,q}\gamma(p,q,k)}{M}. \tag{5}$$

Repeat the above procedure until the results converge. Then, we apply the results into the optical intensity PDF by (2), which is parameterized by model parameters a_i, b_i, c_i, d_i and e_i in the proposed model $I(\theta,\phi)$ by (1). Continuing optimization of (3), the model parameters can be solved by nonlinear regression based on some software packages [21].

2.3 Numerical Fitting and Modeling Performance

The PDF of a measured set of $I(\theta,\phi)$ when $\alpha=180°$ is depicted by dots and compared against the model by solid line in Fig. 3. The number of components K is typically chosen to start and increase from 3. We found $K=6$ is good enough and the excellent agreement is observed.

We define the root mean square error (RMSE) and the R-square to evaluate the accuracy of reconstructed $I(\theta,\phi)$ by (1). The RMSE is

$$\mathrm{RMSE}=\sqrt{\frac{1}{M}\sum_{p,q}[I(\theta_p,\phi_q)-\hat{I}(\theta_p,\phi_q)]^2}, \tag{6}$$

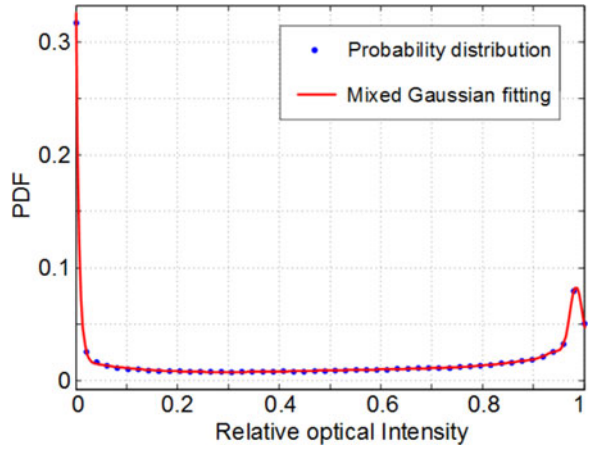

Fig. 3. The PDF of relative optical intensity when $\alpha = 180°$.

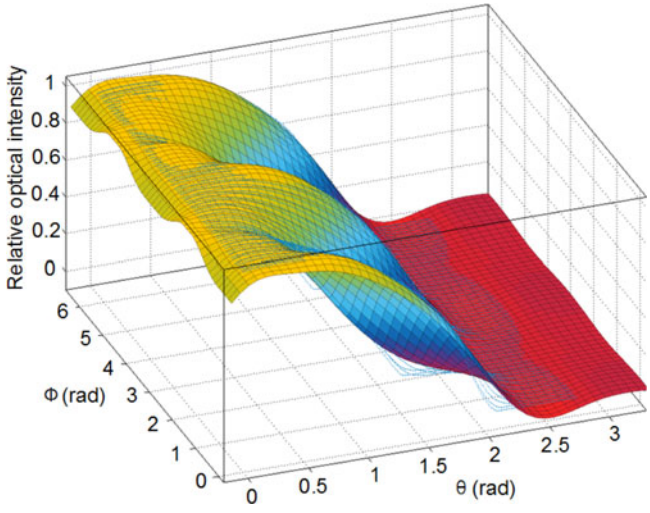

Fig. 4. Comparison between modeled and experimental intensity patterns.

where $I(\theta, \phi)$ is the experimental data and $\hat{I}(\theta, \phi)$ is the modeled data. Generally, the RMSE must be less than the standard error limit of 5% to guarantee enough accuracy [21], [22]. The R-square represents the similarity between the measured pattern and the proposed model, which can be calculated as

$$R - square = \frac{\sum_{p,q}[\hat{I}(\theta_p, \phi_q) - \overline{I}]^2}{\sum_{p,q}[I(\theta_p, \phi_q) - \overline{I}]^2}, \tag{7}$$

where $\overline{I}$ is the mean of experimental data. The R-square should be higher than 99% to provide sufficient accuracy for many applications.

Fig. 4 illustrates an example of $\alpha = 180°$. It shows three-dimensional intensity patterns, where blue dots represent original data. The numerical fitting results of the model parameters up to order $U = 3$ are recorded in Table 1. By increasing U beyond 3, the model accuracy does not increase much. The RMSE is 2.8% and the R-square is 99.48%, which demonstrate that the proposed analytic representation can fit experimental data well. The modeled three-dimensional radiation patterns from different directions in polar coordinates are described in Fig. 5(a) and (b).

TABLE 1
Model Parameters

i	1	2	3
a_i	−0.2573	0.9888	0.113
b_i	2.324	0.5675	−0.03784
c_i	0.486	1.5	0.3064
d_i	1.545	−0.2541	0.6146
e_i	1.023	1.849	0.5223

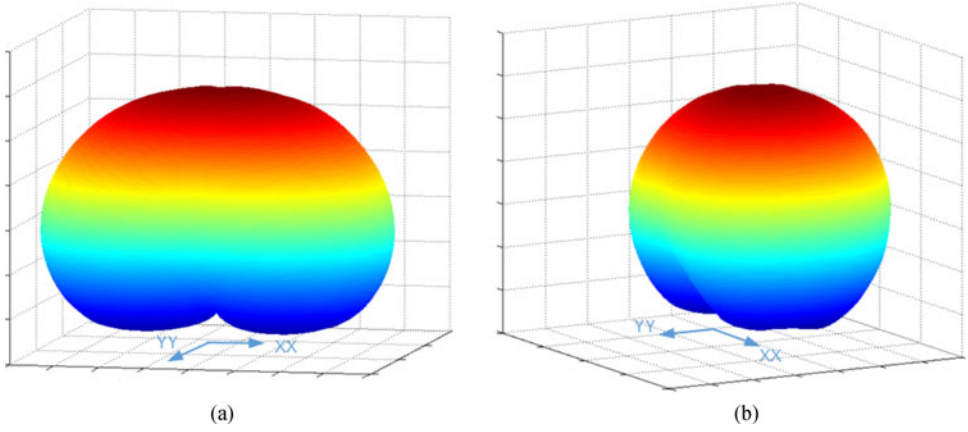

Fig. 5. (a) and (b) Modeled three-dimensional radiation patterns viewed from different angles.

The above radiation pattern model we developed will be applied to subsequent study on the characteristics of the OLED based VLC channel.

3. OLED-Based VLC Channel Characteristics

A typical indoor scenario is depicted in Fig. 6. The light source is fixed on the centre of the ceiling. The normal of the source is vertically downwards. Three typical positions of the receiver on the floor are set in the central, side, and corner of the floor. The key parameters for channel characteristics simulation are consistent with the setting of [15], [23], [24], as Table 2 shows. The size of the room is 5 m × 5 m × 3 m. The reflectance of the ceiling, walls and floor takes 0.8, 0.8 and 0.3 respectively. We build a rectangular coordinate system with the central position of the floor as the origin. The coordinates of light source and three receiver locations are (0,0,3) m, (0,0,0) m, (2.5,0,0) m and (2.5, −2.5,0) m. The field of view (FOV) of the receiver is 85° and the detection area is 1 cm^2. In addition to the three typical receivers, there are 625 receiver positions in total on the floor. The space between two neighbouring receiver positions is 0.2 m.

In an indoor environment, optical signals transmit from light source to the receiver via line of sight (LOS) or reflection paths. The RMS delay spread from the impulse response and optical path loss are adopted to characterize the VLC channel. They are obtained by iterative ray tracing techniques, described in detail in [15]. According to [15], we mainly consider LOS path and the first order reflection paths as the effects from higher order reflection paths are negligibly small.

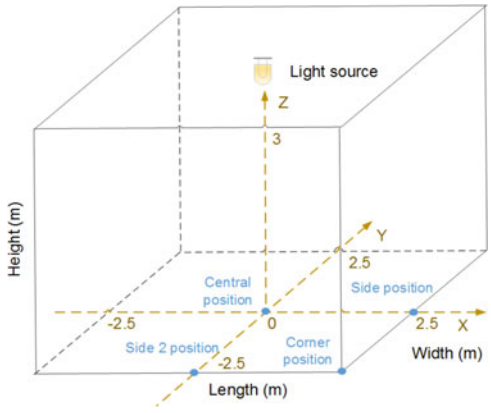

Fig. 6. Indoor scene with a light source and typical receiver positions.

TABLE 2
Parameters for Channel Characteristics Simulation

Parameters	Value
Rome size	5 m × 5 m × 3 m
Reflectance of ceiling	0.8
Reflectance of wall	0.8
Reflectance of floor	0.3
Time resolution	0.2 ns
Reflective element size	0.05 m × 0.05 m
Light source power	1 W
Coordinates of light source	(0,0,3) m
Coordinates of receiver central position	(0,0,0) m
Coordinates of receiver side position	(2.5,0,0) m
Coordinates of receiver corner position	(2.5, −2.5,0) m
Detection area of the receiver	1 cm^2
Fov of the receiver	85°
Spacing of neighbouring receiver positions	0.2 m
Number of receiver positions	625 (25 × 25)

In the following, we compare the OLED panel model with the generalized Lambertian pattern and evaluate the multipath channel performance in terms of RMS delay spread and OPL.

3.1 Root Mean Square (RMS) Delay Spread

The RMS delay spread (σ_τ) is defined to evaluate the multipath dispersion in a VLC system [25]. It can be approximatively expressed based on the channel impulse response $h(t)$ as

$$\sigma_\tau = \left[\frac{\int (t-\mu)^2 h^2(t) dt}{\int h^2(t) dt} \right]^{\frac{1}{2}}, \tag{8}$$

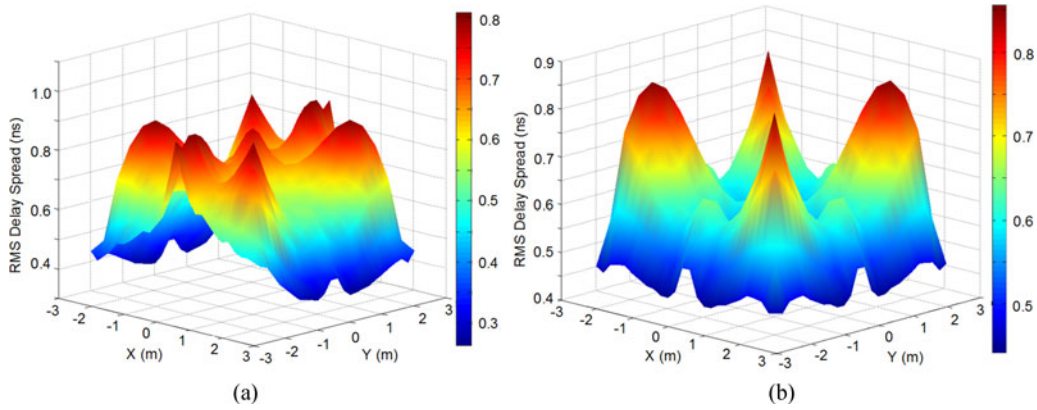

Fig. 7. RMS delay spread distribution of (a) the OLED and (b) the Lambertian source.

where the mean excess delay μ can be computed by $\mu = \frac{\int th^2(t)dt}{\int h^2(t)dt}$. When the RMS delay spread is larger than the symbol duration, ISI occurs and the bit error rate performance will significantly degrade.

The results of RMS delay spreads on the X-Y receiving plane are showed in Fig. 7. For the OLED, the RMS delay spreads along the XX cross section are relatively small with a minimum value at 0.3325 ns. The high values of σ_τ appear at four corners and the left two sides. In these positions, the receiver captures less LOS signal because the distance to the source is far and the radiation intensity at these directions is weak. For the Lambertian source, the profile of the RMS delay spread is symmetric with obvious bulges in four corner positions. The maximum, average, and minimum RMS delay spreads of the OLED are 0.8321 ns, 0.5457 ns, and 0.3325 ns respectively, which are less than those of the Lambertian source (0.8558 ns, 0.5983 ns, and 0.4416 ns) with 2.8%, 8.8%, and 24.7% decreases respectively. It means that the OLED source can provide better communication channel conditions in some specific directions.

3.2 Optical Path Loss (OPL)

In a VLC system, the OPL is an important indicator to evaluate the optical signal attenuation caused by reflections and transmission in the free space [15], [24]. The required emitting power of light source depends on the channel OPL and the detector sensitivity. The OPL can be calculated by the logarithm of the direct current (DC) value of the channel frequency response and is expressed in optical dB (dBo) as

$$L_{OPL} = -10 \log H(0), \tag{9}$$

where the DC gain is obtained by integrating the channel impulse response, i.e. $H(0) = \int h(t)dt$.

Fig. 8 plots the OPL distributions of the two light sources on the receiving plane. We can see that the value of the OPL increases from the center of the X-Y plane to the surrounding areas. The profile of the OPL distribution of the Lambertian source is circular, which indicates that this radiation pattern emanates uniformly along the normal axis. For the OLED panel, the OPL distribution profile presents elliptic. The long axis of the ellipse on the XX cross section corresponds to the axes along which the OLED panel is bent. The maximum, average, and minimum OPL of the OLED-based channel are 57.7574 dBo, 43.9824 dBo, and 40.052 dBo respectively, less than those of the Lambertian source (60.5945 dBo, 46.471 dBo, and 41.768 dBo). There is an improvement of approximately 3 dBo in the average OPL of the OLED-based channel, which can help to reduce the light source power of a VLC system. Moreover, better mobility can be provided to the receiver due to the more uniform coverage performance of the OLED.

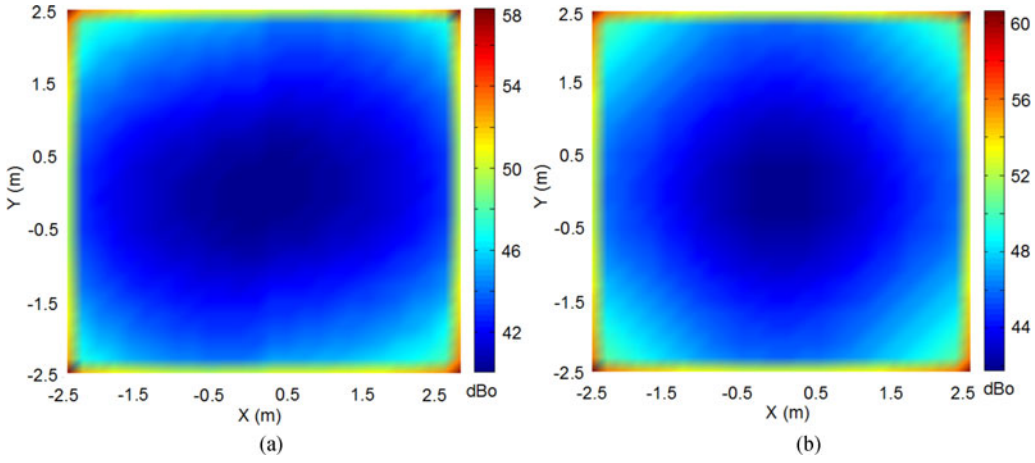

Fig. 8. Optical path loss of (a) the OLED and (b) the Lambertian source.

4. Conclusion

In this paper, we test and model the radiation pattern of a bent OLED panel for the first time. As it no longer presents a Lambertian radiation pattern, we propose an improved analytic representation to describe the rotational asymmetry of the light emitted from the source. We further study the channel RMS delay spread and OPL. The OLED has a broader irradiation range, and can bring better channel performance. Both the RMS delay spread and the OPL of the OLED-based channel are less than those of the Lambertian pattern.

References

[1] H. L. Minh, Z. Ghassemlooy, A. Burton, and P. A. Haigh, "Equalization for organic light emitting diodes in visible light communications," in *Proc. IEEE GLOBECOM Workshop*, Dec. 2011, pp. 828–832.
[2] H. Chun, C. J. Chiang, A. Monkman, and D. O. Brien, "A study of illumination and communication using organic light emitting diodes," *IEEE J. Lightw. Technol.*, vol. 31, no. 22, pp. 3511–3517, Nov. 2013.
[3] P. A. Haigh, Z. Ghassemlooy, S. Rajbhandari, and I. Papakonstantinou, "Visible light communications using organic light emitting diodes," *IEEE Commun. Mag.*, vol. 51, no. 8, pp. 148–154, Aug. 2013.
[4] W. Li *et al.*, "Squarylium and rubrene based filterless narrowband photodetectors for an all-organic two-channel visible light communication system," *Org. Electron.*, vol. 37, pp. 346–351, Oct. 2016.
[5] P. Chvojka, P. Dvorak, P. Pesek, S. Zvanovec, P. A. Haigh, and Z. Ghassemlooy, "Characterization of the organic LED based visible light communications," in *Proc. 10th Int. Symp. Commun. Syst., Netw. Digit. Signal Process.*, Prague, Jul. 20–22, 2016, pp. 1–4.
[6] H. Chen *et al.*, "A 1.9 Mbps OFDM-based all-organic visible light communication system," in *Proc. IEEE Int. Conf. Commun. Syst.*, Dec. 2016, pp. 1–6.
[7] P. A. Haigh, Z. Ghassemlooy, and I. Papakonstantinou, "1.4-mb/s white organic LED transmission system using discrete multitone modulation," *IEEE Photon. Technol. Lett.*, vol. 25, no. 6, pp. 615–618, Feb. 2013.
[8] P. A. Haigh, Z. Ghassemlooy, and H. L. Minh, "Exploiting equalization techniques for improving data rates in organic optoelectronic devices for visible light communications," *IEEE J. Lightw. Technol.*, vol. 30, no. 19, pp. 3081–3088, Oct. 2012.
[9] P. A. Haigh *et al.*, "A MIMO-ANN system for increasing data rates in organic visible light communications systems," in *Proc. IEEE Int. Conf. Commun.*, Jun. 2013, pp. 5322–5327.
[10] S. T. Le *et al.*, "10 Mb/s visible light transmission system using a polymer light-emitting diode with orthogonal frequency division multiplexing," *Opt. Lett.*, vol. 39, no. 13, pp. 3876–3879, Jul. 2014.
[11] P. A. Haigh *et al.*, "A 10 Mb/s visible light communication system using a low bandwidth polymer light-emitting diode," in *Proc. 9th Int. Symp. Commun. Syst. Netw. Digital Signal Process.*, Jul. 2014, pp. 999–1004.
[12] P. A. Haigh *et al.*, "A 20-Mb/s VLC link with a polymer LED and a multilayer perceptron equalizer," *IEEE Photon. Technol. Lett.*, vol. 26, no. 19, pp. 1975–1978, Jul. 2014.
[13] P. A. Haigh *et al.*, "Wavelength-multiplexed polymer LEDs: Towards 55 Mb/s organic visible light communications," *IEEE J. Sel. Areas Commun.*, vol. 33, no. 9, pp. 1819–1828, Sep. 2015.
[14] H. Chen, Z. Xu, Q. Gao, and S. Li, "A 51.6 Mbps experimental VLC system using a monochromic organic LED," *IEEE Photon. J.*, to be published.
[15] J. Ding, L. Chih, and Z. Xu, "Indoor optical wireless channel characteristics with distinct source radiation patterns," *IEEE Photon. J.*, vol. 8, no. 1, pp. 1–15, Dec. 2015.

[16] I. Moreno and C. Sun, "Modeling the radiation pattern of LEDs," *Opt. Express*, vol. 16, no. 3, pp. 1808–1819, Jan. 2008.
[17] A. P. Dempster, N. M. Laird, and D. B. Rubin, "Maximum likelihood from incomplete data via the EM algorithm," *J. Roy. Stat. Soc. B.*, vol. 39, no. 1, pp. 1–38, 1977.
[18] J. Grubor, S. Randel, K.-D. Langer, and J. W. Walewski, "Broadband information broadcasting using LED-based interior lighting," *IEEE J. Lightw. Technol.*, vol. 26, no. 24, pp. 3883–3892, Dec. 2008.
[19] E. F. Schubert, J. K. Kim, H. Luo, and J. Xi, "Solid-state lightinga benevolent technology," *Rep. Prog. Phys.*, vol. 69, no. 12, pp. 3069–3099, Nov. 2006.
[20] C. Sun, C. Lin, T. Lee, and T. Yang, "Enhancement of light extraction of GaN-based light-emitting diodes with a microstructure array," *Opt. Eng.*, vol. 43, no. 8, pp. 1700–1701, Apr. 2004.
[21] C. Daniel and F. S. Wood, *Fitting Equations to Data: Computer Analysis of Multifactor Data*," New York, NY, USA: Wiley, 1999.
[22] W. Chien, C. Sun, and I. Moreno, "Precise optical model of multi-chip white LEDs," *Opt. Express*, vol. 15, no. 12, pp. 7572–7577, Jun. 2007.
[23] J. Ding, K. Wang, and Z. Xu, "Impact of LED array simplification on indoor visible light communication channel modeling," in *Proc. 9th Int. Symp. Commun. Syst. Netw. Digital Signal Process.*, Jul. 2014, pp. 1159–1164.
[24] J. R. Barry, J. M. Kahn, W. J. Krause, E. A. Lee, and D. G. Messerschmitt, "Simulation of multipath impulse response for indoor wireless optical channels," *IEEE J. Sel. Areas Commun.*, vol. 11, no. 3, pp. 367–379, Apr. 1993.
[25] S. Jovkova and M. Kavehard, "Multispot diffusing configuration for wireless infrared access," *IEEE Trans. Commun.*, vol. 48, no. 6, pp. 970–978, Jun. 2000.